Journal of Applied and Computational Mechanics, Vol. 1, No. 4, (2015), 229-239
DOI: 10.22055/jacm.2016.12006


Journal of
Applied and Computational Mechanics

# Pull-in behavior of a bio-mass sensor based on an electrostatically actuated cantilevered CNT with consideration of rippling effect

**Nazanin Farjam**[1]

[1]Mechanical Engineering Department, Faculty of Engineering, Shahid Chamran University of Ahvaz
Ahvaz, Iran, nazanin.farjam@gmail.com

Received April 28 2016; revised June 02 2016; accepted for publication June 10 2016.
Corresponding author: Nazanin Farjam, nazanin.farjam@gmail.com

**Abstract**

This paper examines the pull-in behavior of a bio-mass sensor with a cantilevered CNT actuated electrostatically by considering rippling deformation. Although this phenomenon can remarkably change the behavior of CNT, its effect on the performance of a CNT-based mass sensor has not been investigated thus far. This investigation is based on modified Euler-Bernoulli beam theory and rippling effect is entered into the equations related to the cantilevered CNT-bases sensor. The impact of other properties like different masses, mechanical damping and intermolecular force is studied in this paper, as well. The results reveal that rippling deformation decreases the pull-in voltage and tip deflection of CNT but enhances the pull-in time. Results related to the impact of other mentioned properties are presented, too. The results are compared with other pull-in sensor equations in the literature and "molecular dynamics", in both of which an excellent agreement is seen, to verify the soundness of this study.

**Keywords**: Bio-mass sensor, Rippling Deformation, CNT, Pull-in instability.

## 1. Introduction

Contrary to their simple appearance and geometry, Carbon nanotubes (CNTs) have very exclusive physical and mechanical properties. Due to these properties, they have been recently used in the structure of nano electromechanical systems (NEMS) [1-4]. Nano and bio sensors are examples of such systems [5, 6]. There are different approaches to investigate the dynamic behavior of CNTs. One of these approaches is to carry out an experiment which is so hard to handle in nano dimensions. A second way is molecular dynamic simulation which is highly accurate but limited to the geometry of carbon nanotubes [7]. In continuum modelling, another approach, the behavior of CNTs is investigated based on continuum mechanics theories. It is a proved fact that the results obtained through this simulation are in full agreement with the experimental data [8, 9]. As seen in Figure 1, carbon nanotubes with electrostatic actuation include two conductive electrodes with an initial gap in between, and potential difference applied to them. This difference in potentials leads to the movement of the CNT toward the bottom electrode. The more the potential difference, the more the nanotube moves downward until it touches the bottom electrode. This value of voltage, which is the maximum one for such systems, is called pull-in voltage. Even an epsilon increase in this value breaks the device [10, 11].

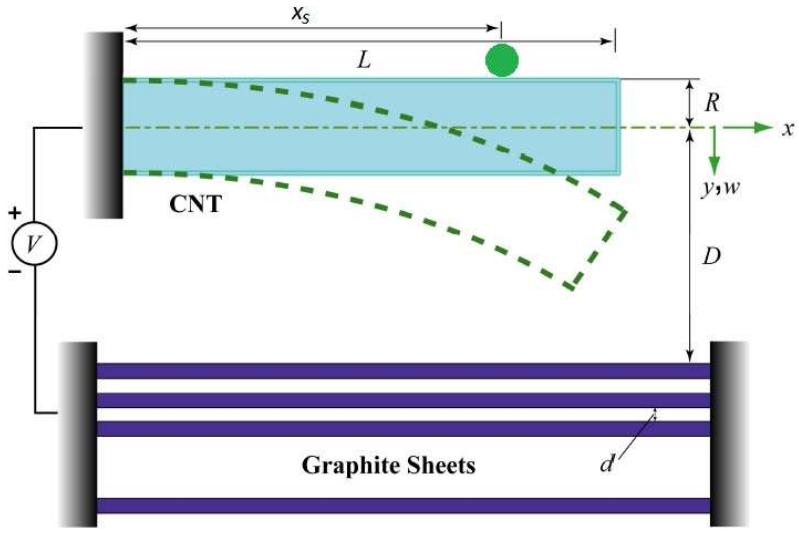


**Fig. 1.** Cantilever CNT actuator as a mass sensor with an attached mass at x=$x_s$.

Rasekh and Khadem investigated non-linear behavior of cantilevered CNT with electrostatic actuation, using Euler-Bernoulli beam theory [12]. In another study, Dequesnes examined the behavior of electrostatically actuated cantilevered CNT, using a combination of molecular dynamics and continuum mechanics approaches [13]. As stated earlier, specific properties of CNTs entered them to the construction of nano-sensors. In mass sensors, the resonance frequency of the resonator is dependent on the mass attached to it; hence, the value and the location of mass change the resonance frequency. Mehdipour et al. [14] investigated the pull-in behavior of a CNT-based bio-mass sensor by using nonlocal Euler-Bernoulli beam theory. CNTs, due to their remarkable flexibility, can tolerate large deformations in bending without fracture. In such situations, a phenomenon called rippling deformation occurs in a way that ripples are created on the inner arc of the CNT. Rippling deformation considerably affects the bending behavior of CNTs, which is so significant in the precise design of them. However, none of the classical theories can describe this phenomenon since once rippling deformation is considered, the relationship between bending moment and curvature is no longer linear. Wang et al. [15] achieved this relationship in the presence of rippling deformation, showing that the relationship of bending stiffness and CNT deformation is certainly nonlinear. Soltani [16] studied a nonlinear continuum elastic model based on rippling deformations and analyzed the transverse vibration of carbon nanotubes embedded on a Winkler elastic foundation. Nonetheless, the effect of rippling deformation on instability actuation of nano-mass sensors has not been investigated thus far.

## 2. Statement of the problem and governing equation

In this section, we attempt to state the problem and obtain the governing equation by considering rippling deformation, vdW force and mechanical damping. Figure 1 shows the problem schematically. The nano-sensor includes two electrodes, one of which is a cantilevered CNT with length of $L$ and the mean Radius of $R_w$ and wall layers of $N_w$ and the other is the graphite sheets with a gap of $d$ between every two sheets. There is an initial gap between these two electrodes ($D$). As mentioned above, the voltage ($V$) applied to them results in the movement of the CNT toward the graphite sheets.

The equation of vibration of a CNT with consideration of rippling effect can be expressed as:

$$\frac{\partial^2 M}{\partial x^2} + c\frac{\partial w}{\partial t} + \rho A\frac{\partial^2 w}{\partial t^2} = q(x,t) \tag{1}$$

where $M(x,t)$ is the bending moment of the nanotube, $c$ is the mechanical damping, $w(x,t)$ the CNT transverse displacement, $\rho$ the density of nanotube material, $A$ the cross-sectional area of the CNT and $q(x,t)$ the distributed force per unit length of the CNT, which is written as [17,18]:

$$q(x,t) = q_{vdW} + F_e = \frac{C_6\sigma^2\pi^2 N_w R_w}{d(D-w)^4} + \frac{\pi\varepsilon_0 V^2}{\sqrt{(D-w)(D-w+2R_w)}\,(cosh^{-1}\left(\frac{D-w}{R_w}\right))^2} \tag{2}$$

where $q_{vdw}$ is the intermolecular force per unit length of CNT, $F_e$ represents the electrostatic force, $C_6 = 15.2eV\text{Å}^6$ is the attractive constant for the carbon-carbon interaction and $\varepsilon_0 = 8.854\times10^{-12}C^2N^{-1}m^{-2}$ is the permittivity of vacuum. As stated earlier on, the relationship found between bending moment and curvature of the CNT is nonlinear when the rippling deformation is taken into account. It is expressed as [15]:

$$M(x,t) = EIK(1 - a_3{D_w}^2K^2 + a_5{D_w}^4K^4 - a_7{D_w}^6K^6 + a_9{D_w}^8K^8) \tag{3}$$

$$K(x,t) = \frac{w''(x,t)}{[1+w'(x,t)^2]^{3/2}} = w''[1 - \frac{3}{2}(w')^2 + \frac{15}{8}(w')^4 - \cdots] \cong w''(x,t)[1 - r(w')^2] \tag{4}$$

where $E$ is the Young's modulus, $I$ the second moment of the cross-sectional area, $K$ the curvature of CNT and $D_w$ represents the mean diameter of nanotube. By using equation 3, the second partial derivative of bending moment is obtained. Next, by substituting the second derivative and equation 2 in equation 1 and then making it non-dimensional, we will have:

$$W = \frac{w}{D} \text{ ، } x^* = \frac{x}{L} \text{ ، } t^* = \frac{t}{L^2}\sqrt{\frac{EI}{\rho A}} \text{ ، } \xi = \frac{x_s}{L} \tag{5a}$$

$$W'''' - \frac{12a_3b^4}{k^2}[2W''(W''')^2 + (W'')^2W''''] - rb^2[2(W'')^3 + 6W'W''W''' + (W')^2W''''] + C\dot{W} + \ddot{W} = \frac{\delta V^2}{\sqrt{(1-W)\left(1-W+\frac{2}{k}\right)\left(\cosh^{-1}\left(1+k(1-W)\right)\right)^2}} + \frac{f}{k(1-W)^4} \tag{5b}$$

in which non-dimensional parameters are expressed as:

$$\frac{D}{R_w} = k \text{ ، } \frac{D}{L} = b \text{ ، } f = \frac{C_6\sigma^2\pi^2N_w}{db^4EI} \text{ ، } \delta = \frac{\pi\varepsilon_0L^4}{EID^2} \text{ ، } C = cL^2\sqrt{\frac{1}{\rho AEI}} \tag{6}$$

where prime and dot represents the derivatives with respect to $x^*$ and $t^*$, respectively.

## 3. Numerical solution

Glarkin approach should be used in order to separate the variables. Therefore, the non-dimensional deflection is written as [19]:

$$W(x,t) = \sum_{i=1}^{\infty} q_i(t)\phi_i(x) \tag{7}$$

in which $q_i$ is the dynamic response of the CNT and $\phi_i$ is the ith linear mode shape of the uninflected cantilever-beam which is considered as:

$$\phi_i(x) = cosh(\beta_i x) - cos(\beta_i x) - \alpha_i(sinh(\beta_i x) - sin(\beta_i x)) \quad , i = 1,2,3,\ldots \tag{8a}$$

$$\alpha_i = \frac{cosh(\beta_i) + cos(\beta_i)}{sinh(\beta_i) + sin(\beta_i)} \tag{8b}$$

And the values of $\beta_i$ quantities are the roots of the characteristic equation which are obtained in Ref. [14] and its values can be seen in Table 1.

**Table 1.** Values of $\boldsymbol{\beta}$ for different masses attached to the CNT [14]

| Mass (fg) | ξ=0.1 | ξ=0.5 | ξ=1 |
|---|---|---|---|
| **0** | 1.8755 | 1.8755 | 1.8755 |
| **$10^{-8}$** | 1.8755 | 1.8755 | 1.8745 |
| **$10^{-7}$** | 1.8755 | 1.8745 | 1.8685 |
| **$10^{-6}$** | 1.8755 | 1.8675 | 1.8135 |
| **$10^{-5}$** | 1.8745 | 1.8045 | 1.4995 |
| **$10^{-4}$** | 1.8735 | 1.4545 | 0.9435 |
| **$10^{-3}$** | 1.8545 | 0.8965 | 0.5385 |
| **$10^{-2}$** | 1.5955 | 0.5095 | 0.3035 |

Since this function is orthogonal, the following relationship is established:

$$\int_0^l \phi i(x)\phi j(x)dx = \begin{cases} 1 & i = j \\ 0 & i \neq j \end{cases} \tag{9}$$

By substituting Eq. (7) into in the governing equation of motion, Eq. (5b), followed by multiplying the obtained equations by the mode shape, $\phi_1(x)$, and integrating from 0 to 1, a set of coupled nonlinear ordinary differential equations are obtained:

$$\beta_1{}^4 q_1(t) - M q_1(t)^3 + C\dot{q}_1(t) + \ddot{q}_1(t) = H \tag{10a}$$

where

$$H = \delta \int_0^1 \frac{V^2 \phi_1(x)}{\sqrt{\left(1 - q_1(t)\phi_1(x)\right)\left(1 - q_1(t)\phi_1(x) + \frac{2}{k}\right)}\left(cosh^{-1}\left(1 + k\left(1 - q_1(t)\phi_1(x)\right)\right)\right)^2} dx + \int_0^1 \frac{f\phi_1(x)}{k\left(1 - q_1(t)\phi_1(x)\right)^4} dx$$

$$M = \frac{12 a_3 b^4}{k^2}\left[2\int_0^1 \phi_1(x)\phi_1{}''(x)\left(\phi_1{}'''(x)\right)^2 dx + \beta_1{}^4 \int_0^1 \left(\phi_1{}''(x)\right)^2 \phi_1{}^2(x)\, dx\right] + rb^2[2\int_0^1 \phi_1(x)\left(\phi_1{}''(x)\right)^3 dx + 6\int_0^1 \phi_1(x)\phi_1{}'(x)\phi_1{}''(x)\phi_1{}'''(x)\, dx + \beta_1{}^4 \int_0^1 \left(\phi_1{}'(x)\right)^2 \phi_1{}^2(x)\, dx] \tag{10b}$$

As can be seen, terms of the equation including electrostatic and vdW force are nonlinear. As a solution for this problem, we have to solve it numerically by separating the range of location and using numerical approaches for numerical integration. The point is that it should be done in a time step before. In order to solve the time differential equation in terms of $q$, this integration should be entered the equations as input from the previous step, in a way that the response in the right side of the equation is entered the equation as input for the next step, and the obtained equation can be solved in each interval by means of numerical integration approaches similar to trapezoidal integration. The shorter the intervals, the more accurate the response of the equation would be.

## 4. Numerical Results

### 4.1 Verification

The results obtained from presented simulation and method are compared with those obtained in Ref. [12] for different values of $b$ with the aim of validating the present study.

**Table 2.** Comparisons between obtained results and results of Ref. [12]

| b | Ref[12] | Present study |
|---|---|---|
| **0.1** | 1.324 | 1.3194 |
| **0.25** | 4.249 | 4.2378 |
| **0.5** | 10.19 | 10.164 |
| **0.75** | 16.905 | 16.589 |

As another comparison, the results of the present study are compared with the published results using molecular dynamics [6] (see Figure 2). As can be observed, considering rippling deformation, results are remarkably close to those obtained through a molecular dynamics method. Physical properties for this comparison can be seen if Ref. [6]. To sum up, these two comparisons verify the validity of this analysis.

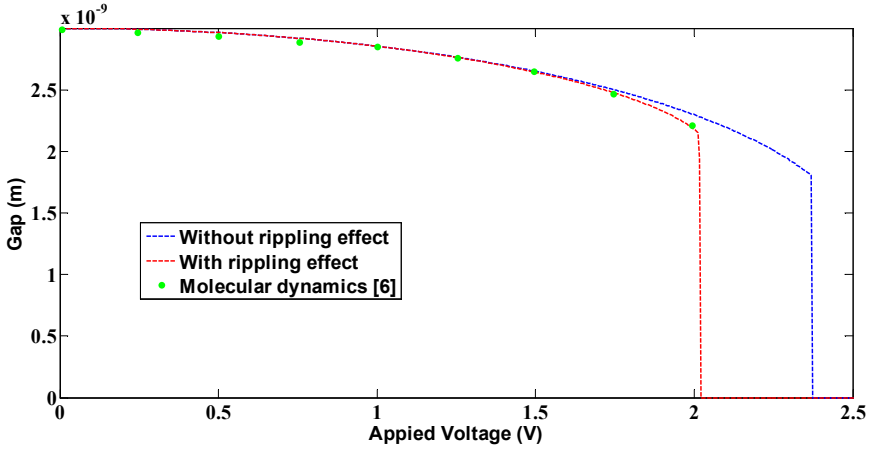


**Fig. 2.** Variation of the gap between CNT and the substrate versus applied voltage as a comparison of different methods.

### 4.2 Results

In the first section, the influence of different masses on instability behavior of the mass sensor is presented. For this purpose, Figure 3 shows the variation of the gap between CNT and substrate versus the applied voltage for

different masses. It is clearly seen that the gap decreases with the increase of the actuation voltage up to the pull-in voltage, where the CNT touches the bottom electrode. According to this figure, it is obviously observed that the effect of mass on the CNT is to reduce the dynamic pull-in voltage of CNT actuators. Put differently, the heavier the mass, the less the pull-in voltage. Furthermore, the variation of the pull-in voltage versus parameter $k$ is shown in Fig. 4. According to this figure, the dynamic pull-in voltage increases with the increase of the gap-radius ratio. In addition, one can observe that the dynamic pull-in value shifts downward as the mass increases on the CNT in the simulation. The duration for CNT to reach the pull-in instability and touch the substrate from initial state is called the pull-in time. The effect of different masses entering the sensor on the dynamic response of actuated CNT-based sensor is displayed in Figs. 5 and 6. It is shown that by increasing the mass, the pull-in time of nanotube and the pull-in deflection at pull-in voltage are enhanced.

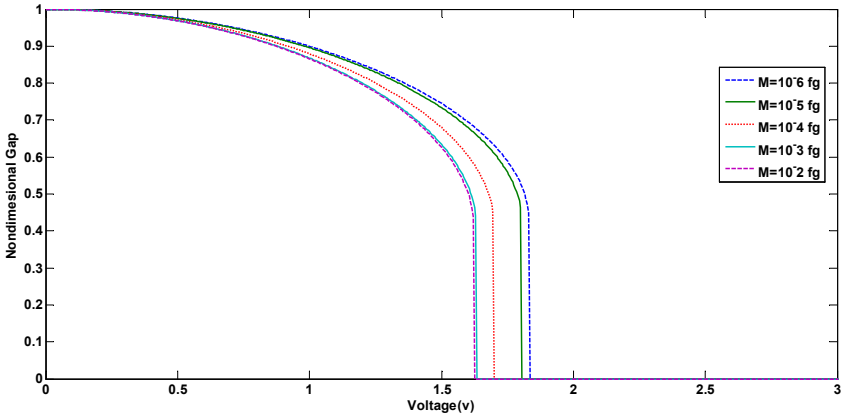


**Fig. 3.** Variation of the gap between CNT and the substrate versus applied voltage for different masses at ξ=0.5.

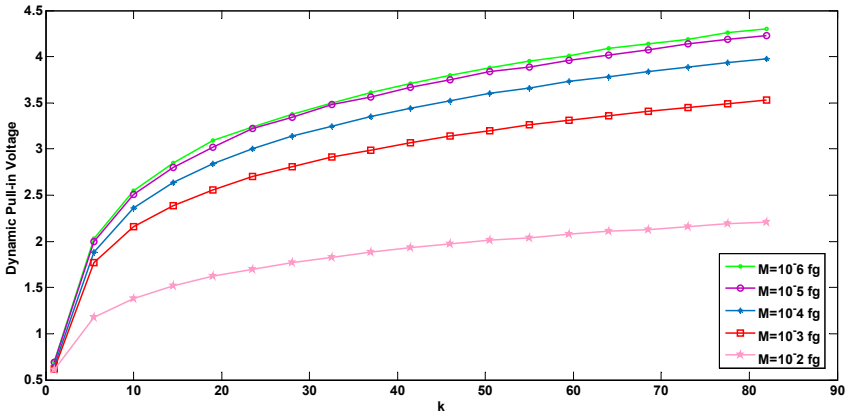


**Fig. 4.** Variation of dynamic pull-in voltage versus parameter k for different masses at ξ=0.5.

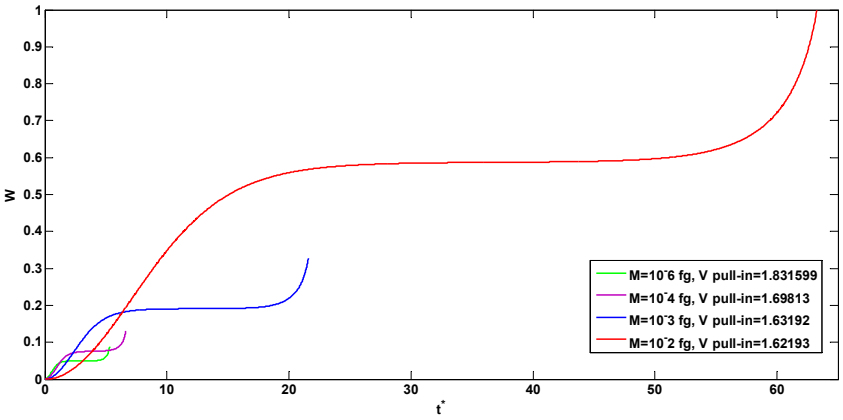


**Fig. 5.** Nondimensional tip deflection time history of CNT for different masses at ξ=0.5.

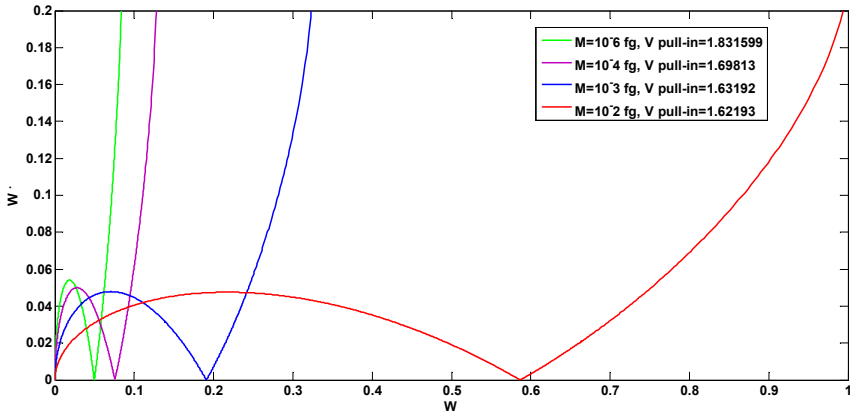


**Fig. 6.** Phase portrait of CNT for different masses at $\xi$=0.5.

In the second part, the influence of rippling deformation is presented. Fig. 7 displays the pull-in voltage of the CNT in the case of non-dimensional gap. This plot indicates that by taking rippling deformation into account, the CNT of the sensor reaches pull-in instability at a lower voltage compared to when this phenomenon is ignored. For more thorough investigation, figures 8 and 9 demonstrate the effect of rippling phenomenon on tip deflection and time history of the CNT. As can be seen, with consideration of rippling deformation the CNT of the sensor takes far more time to reach the pull-in instability at its pull-in voltage in comparison with classical theories. However, in spite of the enhancement in pull-in time, deflection of the CNT decreases remarkably with regard to rippling effect. The results indicate that rippling phenomenon affects the bending behavior of the CNT to a considerable extent.

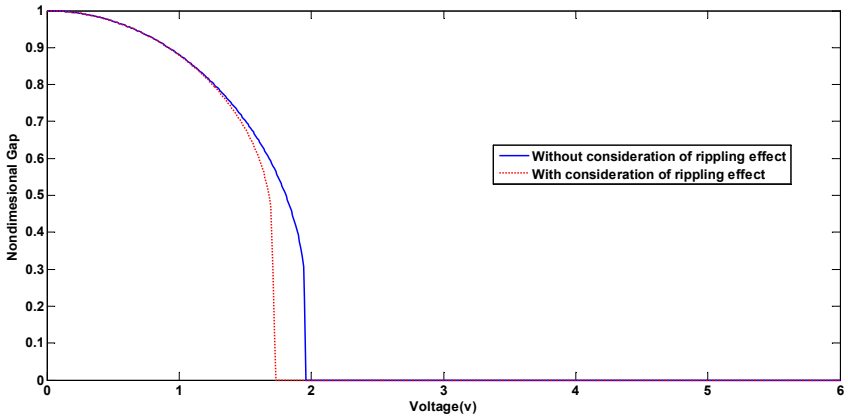


**Fig. 7.** Rippling impact on variation of the gap between CNT and the substrate versus applied voltage for M=$10^{-4}$fg at $\xi$=0.5.

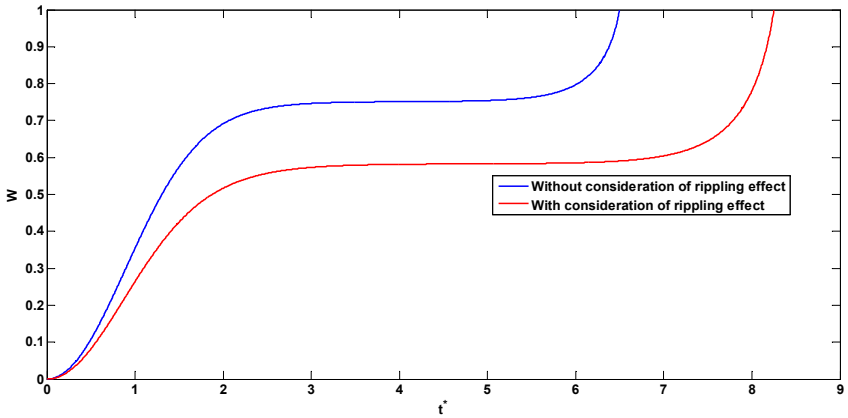


**Fig. 8.** Rippling impact on nondimensional tip deflection time history of CNT for M=$10^{-4}$fg at $\xi$=0.5.

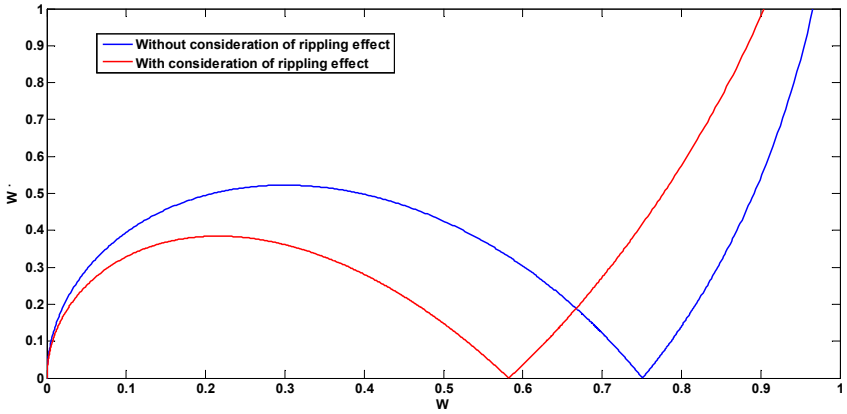


**Fig. 9.** Rippling impact on phase portrait of CNT for M=$10^{-4}$fg at ξ=0.5.

It would be worthwhile to allocate a part to the investigation of damping effect on dynamic behavior of CNT. Fig. 10 depicts the pull-in voltage as a function of gap between CNT and the substrate. According to this figure, as the dynamic damping is taken into account, the pull-in voltage increases. The higher the damping coefficient, the higher the pull-in voltage would be. In addition, Fig. 11 shows the nondimensionel gap versus the gap-radius ratio. Considering this figure, the damping coefficient decreases the gap between CNT and the bottom electrode for a specific *k*, and the magnitude of this decrease depends on the value of c. As Fig. 11 illustrates, this parameter affects the pull-in time and deflection alike. Once damping is considered, the CNT needs much time to reach pull-in instability, and the pull-in deflection is less. Figs. 12 and 13 show that in the absence of damping and for voltages below the pull-in voltage, the CNT tip deflection shows periodic oscillations.

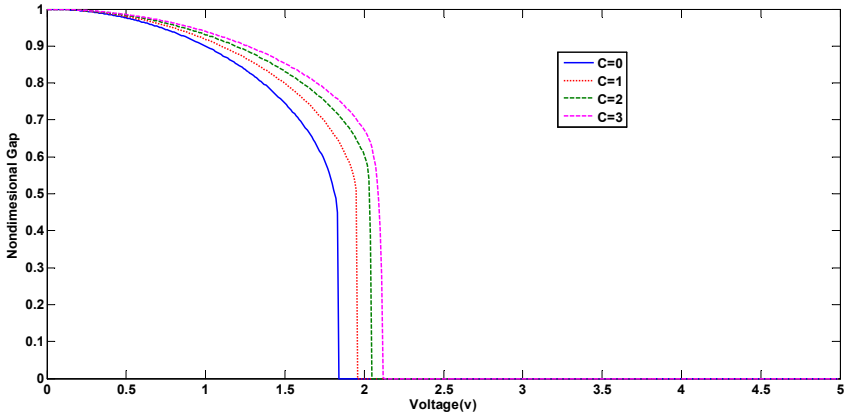


**Fig. 10.** Variation of the gap between CNT and the substrate versus applied voltage (M=$10^{-6}$fg at ξ=0.5) for different *C*s.

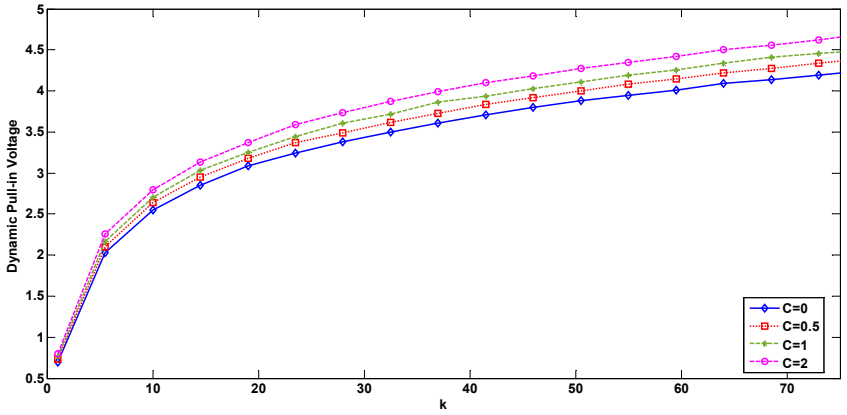


**Fig. 11.** Variation of dynamic pull-in voltage versus parameter k (M=$10^{-6}$fg at ξ=0.5) for different *C*s.

However, in the presence of this property and at a voltage less than the pull-in voltage, the tip deflection is damped gradually until it reaches a steady state (Figs. 14 and 15). Moreover, one can clearly see that even at a voltage an epsilon less than pull-in instability, deflection of CNT tip is periodic. However, at pull-in voltage no

harmonic movement is seen in the behavior of tip deformation and tip shifts downward abruptly until it touches the bottom electrode. Figs. 13 and 15 demonstrate the diagram phase of CNT with and without damping. Fig. 136 reveals circular motions in the absence of damping and at small amounts of voltage in a way that these circles become stretched gradually until pull-in instability is achieved. At the voltage related to the pull-in, a fracture is seen in its graph. In the presence of damping the behavior of CNT is the same. The only difference is that, instead of circular motions, spiral ones are seen in the diagram phase of CNT before instability (Fig. 15). However, afterwards, it behaves just like when c is zero.

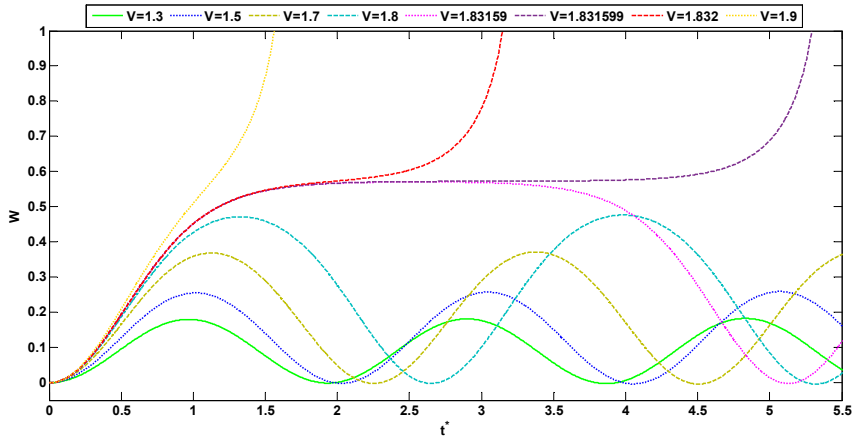


**Fig. 12.** Nondimensional tip deflection time history of CNT ($M=10^{-6}$fg at $\xi=0.5$) in absence of damping for different applied voltages.

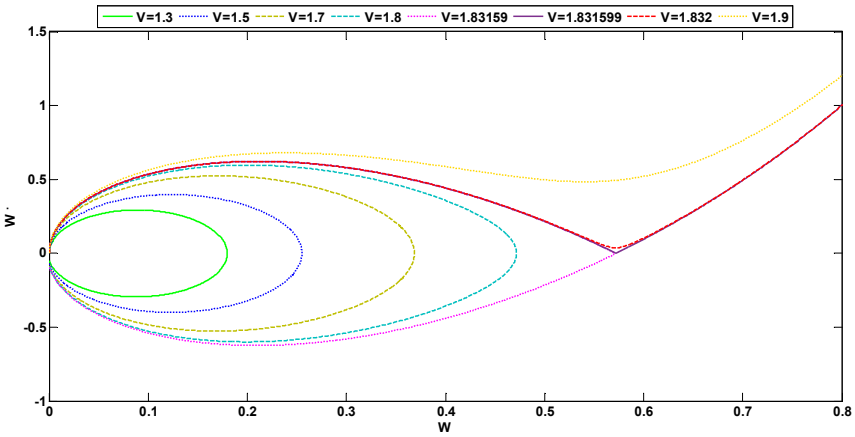


**Fig. 13.** Phase portrait of CNT ($M=10^{-6}$fg at $\xi=0.5$) in absence of damping for different applied voltages.

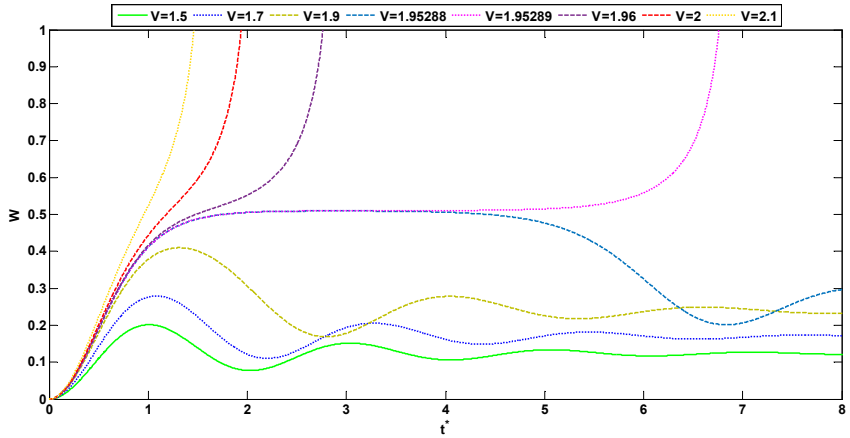


**Fig. 14.** Nondimensional tip deflection time history of CNT ($M=10^{-6}$fg at $\xi=0.5$) in presence of damping for different applied voltages.

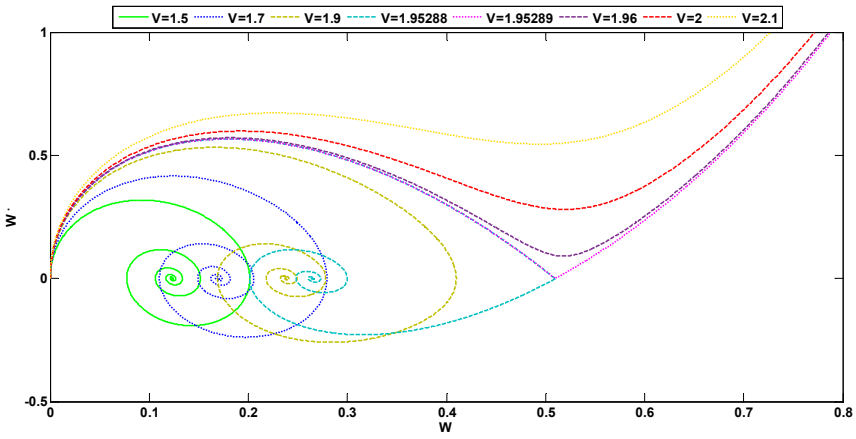


**Fig. 15.** Phase portrait of CNT ($M=10^{-6}$fg at $\xi=0.5$) in presence of damping for different applied voltages.

Finally, we study the impact of intermolecular force on dynamic behavior of CNT. As can be seen from Fig. 16, the more the intermolecular parameter, the less the voltage needed for the CNT in order to reach pull-in instability. For the purpose of more investigation, Fig. 17 is presented. One can clearly see that if intermolecular force is taken into account, tip deflection and its velocity increase.

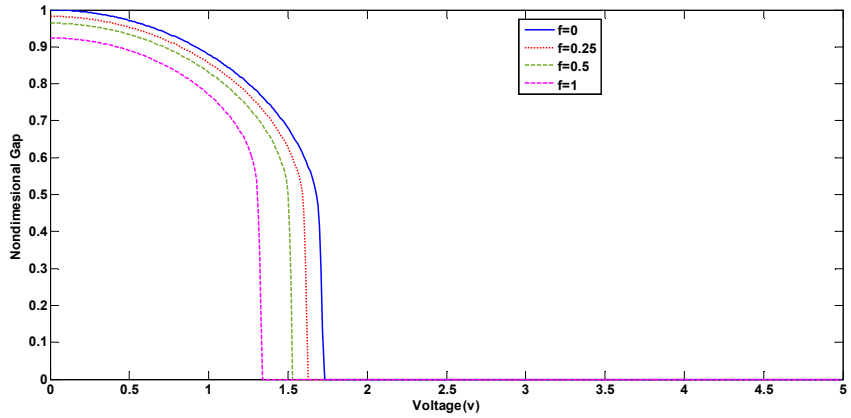


**Fig. 16.** Variation of the gap between CNT and the substrate versus applied voltage ($M=10^{-4}$fg at $\xi=0.5$) for different *f*s.

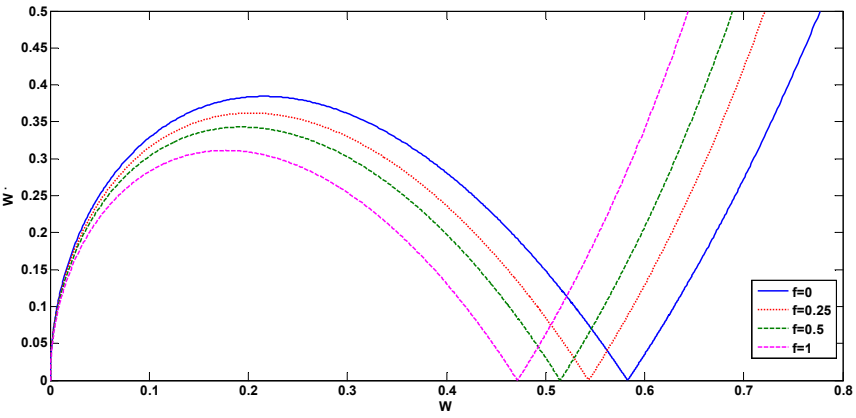


**Fig. 17.** Phase portrait of CNT ($M=10^{-4}$fg at $\xi=0.5$) for different *f*s.

## 5. Conclusions

The present paper examines the pull-in behavior of a bio-mass sensor based on an electrostatically actuated cantilevered CNT by considering rippling effect which is studied in light of the Euler–Bernoulli beam theory. The governing equation including rippling effect terms and numerical method are presented as its solution. The influence of different masses on the CNT, rippling deformation, mechanical damping and van der Waals force is discussed, as

well. From the numerical results analyzed above, the most significant observations are summarized as follows:

1. An excellent agreement is observed between the results of the proposed analysis and the molecular dynamic. This confirms the reliability of the presented approaches.
2. The dynamic pull-in voltages obtained by considering rippling are always smaller than those obtained by the classical theory.
3. The results demonstrate that taking rippling deformation into account, the pull-in time increases while tip deflection related to this time is smaller.
4. Mechanical damping increases the pull-in voltage and time of CNT while it reduces the tip deflection of the CNT.
5. For voltages less than the pull-in voltage, periodic motions are seen in time history and phase diagram of the CNT, whereas at pull-in voltage and for more values of it, the CNT goes downward abruptly and fractures are seen in the relevant phase diagram.
6. The intermolecular force reduces the pull-in voltage and tip deflection of the CNT.

## References


[1] Keivan Kiani, Hamed Ghaffari, Bahman Mehri, Application of elastically supported single-walled carbon nanotubes for sensing arbitrarily attached nanoobjects, *Current Applied Physics* 13 (2013) 107-120.

[2] Ho Jung Hwang, Jeong Won Kang, Carbon-nanotube-based nanoelectromechanical switch, *Physica E: Low-dimensional Systems and Nanostructures* 27 (2005) 163-175.

[3] K. Azizi, S. Majid Hashemianzadeh, Sh. Bahramifar, Density functional theory study of carbon monoxide adsorption on the inside and outside of the armchair single-walled carbon nanotubes, *Current Applied Physics* 11 (2011) 776-782.

[4] Muhammad A. Hawwa, Hussain M. Al-Qahtani, Nonlinear oscillations of a double-walled carbon nanotube, *Computational Materials Science* 48 (2010) 140-143.

[5] S.K. Georgantzinos, N.K. Anifantis, Carbon nanotube-based resonant nanomechanical sensors: a computational investigation of their behavior, *Physica E: Low-dimensional Systems and Nanostructures* 42 (2010) 1795-1801.

[6] M.Z. Atashbar, B. Bejcek, S. Singamaneni, Carbon nanotube based biosensors. *Vienna, Austria, in: IEEE Sensor Conference* (October 24th-27th, 2004), pp.1048-1105.

[7] R.F. Gibson, E.O. Ayorinde, Y.F. Wen, Vibrations of carbon nanotubes and their composites: a review, *Composites Science and Technology* 67 (2007) 1-28.

[8] T. Murmu, S. Pradhan, Thermo-mechanical vibration of a single-walled carbon nanotube embedded in an elastic medium based on nonlocal elasticity theory, *Computational Materials Science* 46 (2009) 854e859.

[9] S. Gupta, R. Batra, Continuum structures equivalent in normal mode vibrations to single walled carbon nanotubes, *Computational Materials Science* 43 (2008) 715-723.

[10] K. Tonisch, V. Cimalla, F. Will, F. Weise, M. Stubenrauch, A. Albrecht, M. Hoffmann, O. Ambacher, Nanowire-based electromechanical biomimetic sensor, Physica E: Low-dimensional Systems and Nanostructures 37 (2007) 208-211.

[11] J. Zhu, Pull-in instability of two opposing microcantilever arrays with different bending rigidities, International Journal of Mechanical Sciences 50 (2008) 55-68.

[12] M. Rasekh, S.E. Khadem, Pull-in analysis of an electrostatically actuated nanocantilever beam with nonlinearity in curvature and inertia, International Journal of Mechanical Sciences 53 (2011) 108-115.

[13] Dequesnes, M., Tang, Z., Aluru, N.R., Static and Dynamic Analysis of Carbon Nanotube-Based Switches,*Journal of Engineering Materials and Technology*, 126(3) (2004) 230-237.

[14] I. Mehdipour, A. Erfani-Moghadam, C. Mehdipour Application of an electrostatically actuated cantilevered carbon nanotube with an attached mass as a bio-mass sensor, *Current Applied Physics* 13 (7), 1463-1469.

[15] Wang, X.Y., Wang, X., Numerical simulation for bending modulus of carbon nanotubes and some explanations for experiment, *Composites: Part B*, 35 (2004) 79–86.

[16] Payam Soltani, D. D. Ganji, I. Mehdipour1 and A. Farshidianfar, Nonlinear vibration and rippling instability for embedded carbon nanotubes, *Journal of Mechanical Science and Technology* 26 (4) (2012) 985-992.

[17] Koochi, A., Kazemi, A.S., Noghrehabadi, A., Yekrangi, A., Abadyan, M., New approach to model the buckling and stable length of multi walled carbon nanotube probes near graphite sheets, *Materials and Design*, 32 (2011) 2949-2955.

[18] Hayt, W.H., Buck, J.A., Engineering electromagnetic, 6th ed. New York: McGrawHill, (2001).

[19] Abbasnejad, B., Rezazadeh, G., Shabani, R., Stability analysis of a capacitive fgm micro-beam using modified couple stress theory, *Acta Mechanica Solida Sinica*, 26(4) (2013) 427-440.